Bioorganic & Medicinal Chemistry Letters 23 (2013) 5155–5164

Contents lists available at ScienceDirect

Bioorganic & Medicinal Chemistry Letters

journal homepage: www.elsevier.com/locate/bmcl

The discovery of inhibitors of Fas-mediated cell death pathway using the combined computational method ☆

Seo Hee Jung [a], Ji Hee Suh [b], Eun Hee Kim [c], Jun Tae Kim [a], Seung-Eun Yoo [a], Nam Sook Kang [a,*]

[a] Graduate School of New Drug Discovery and Development, Chungnam National University, Daehakno 99, Yuseong-gu, Daejeon 305-764, Republic of Korea
[b] Bio-organic Science Division, Korea Research Institute of Chemical Technology, Yuseong-gu, Daejeon 305-600, Republic of Korea
[c] College of Biological Science and Biotechnology, Chungnam National University, Daehakno 99, Yuseong-gu, Daejeon 305-764, Republic of Korea

ARTICLE INFO

Article history:
Received 5 March 2013
Revised 25 June 2013
Accepted 12 July 2013
Available online 19 July 2013

Keywords:
Fas-mediated cell death pathway
Pharmacophore
3D-QSAR

ABSTRACT

In this study, pharmacophore and 3D-QSAR models were developed for analogues of 3-substituted-benzofuran-2-carboxylate as inhibitors of Fas-mediated cell death pathways. Our pharmacophore model has good correspondence with experimental results and can explain the variance in biological activities coherently with respect to the structure of the data set compounds. The predictive power for our synthesized compounds were 0.96 for the pharmacophore model, 0.58 for the comparative molecular field analysis (CoMFA) model, and 0.57 for the comparative molecular similarity analysis (CoMSIA) model.

The contraction or occlusion of blood vessels results in ischemia, which is frequently associated with cardiovascular diseases, angina pectoris, coronary artery diseases, and other heart conditions.[1,2] Recent studies have shown that caspase-independent cell death (CICD) mediators including RIP1K, JNK, and PARP are significant in ischemic cell death.[3] Alternatively, caspase-dependent cell death (CDCD) is also an important alternative pathway for ischemic cell death.[4,5] In particular, Fas-mediated cell death has an important function in CDCD as a component of the Fas-death inducing signaling complex (DISC) and it also sensitizes cells to chemotherapeutics in chemotherapeutics-induced cell death.[4] Following the Fas-DISC formation, caspase-8 is activated, which then triggers programmed cell death, that is, apoptosis.[5] Blocking the Fas-mediated cell death pathway has been reported to be effective in the treatment of ischemic strokes, myocardial hypertrophy, and traumatic brain injuries.

In this study, we optimized the inhibitors of the Fas-mediated cell death pathway screened using pharmacophore and 3D-QSAR models. We built a combined qualitative pharmacophore and 3D-QSAR, comparative molecular field analysis (CoMFA)/comparative molecular similarity analysis (CoMSIA) models of heterocyclic carboxylate derivatives (3-substituted-benzofuran, furo[2,3-*b*]pyridine, thiophene and pyrazole derivatives).[5–9] The pharmacophore model and 3D-QSAR, CoMFA/CoMSIA calculative analyses were performed using Catalyst and Accerlys Discovery Studio 3.1 and Tripos Sybyl 2.0, respectively. All chemical inhibitors and their biological data (e.g., cell death values) were obtained from high-throughput screening experiments including the work in our previous paper.[5] The cell death (%) values ranged from 4.00% to 30.86% for the 32 compounds selected for the theoretical model in this research. The biological activities (EC_{50}) were obtained from the known cell death (%) and EC_{50} data using a simple regression analysis, and then the EC_{50} was converted to pEC_{50} ($=-\log EC_{50}$) in order to obtain useful values. The biological activity values (pEC_{50}) of the training set and test set compounds cover a range of more than 3 log units ($pEC_{50} = 5–7$), as shown in Table 1.

The training set of the pharmacophore model included 7 compounds with high-ranked activity and the remaining 25 compounds were used as a test data set. The common pharmacophore features were applied using the HipHop algorithm in order to generate a qualitative common features model, which was implemented in the Catalyst molecular modeling software.[10,11] Because this algorithm is a useful computational tool for building a 3D pharmacophore, we performed the HipHop pharmacophore modeling using a highly active compound. In the HipHop run, the most active compound (compound **27**) was considered as the reference compound, which specifies a principal value of 2 and a maximum omitted feat (MOF) value of 0. The initial features were specified based on an overview of the training set including the hydrogen-bond donor (HBD), hydrogen-bond acceptor (HBA), ring aromatic feature (RA), and hydrophobic feature (HY).

* Corresponding author.
E-mail address: nskang@cnu.ac.kr (N.S. Kang).

0960-894X/$ - see front matter © 2013 The Authors. Published by Elsevier Ltd. All rights reserved.
http://dx.doi.org/10.1016/j.bmcl.2013.07.018

Table 1
Structure and biological activity of the training and test set

Compound	Structure	pEC_{50}	Compound	Structure	pEC_{50}
1	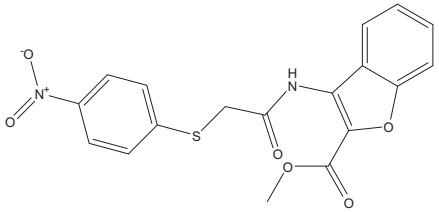	6.24	**17**	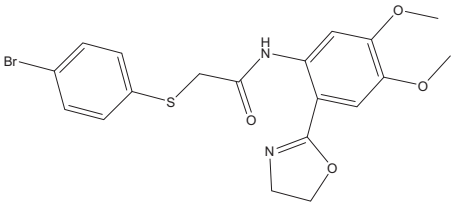	6.02
2	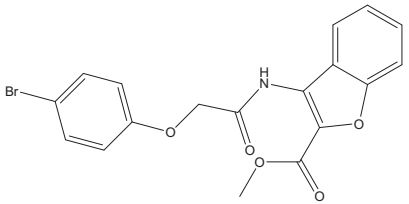	5.98	**18**	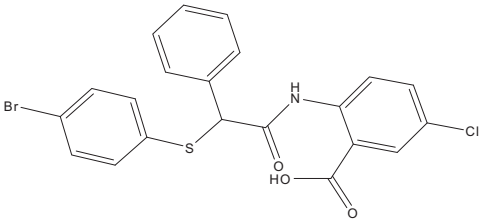	5.70
3	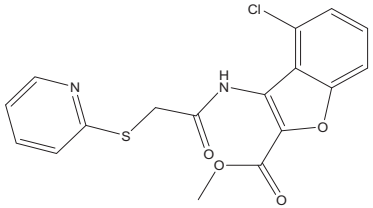	6.19	**19**	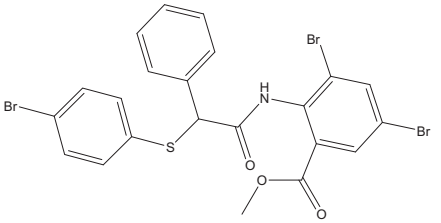	5.80
4	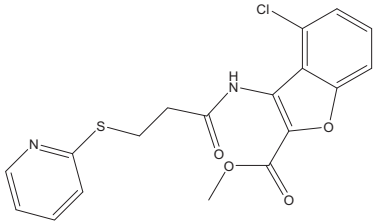	6.20	**20**	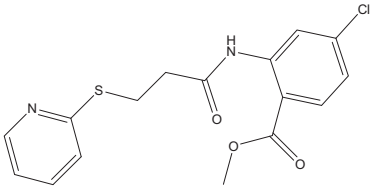	5.99
5	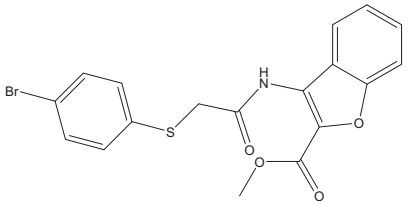	6.18	**21**	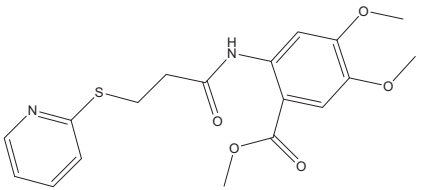	5.88

6	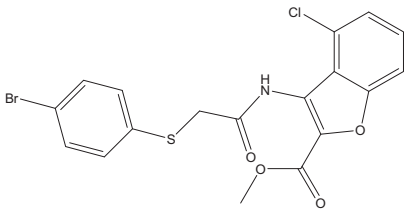	5.94
7	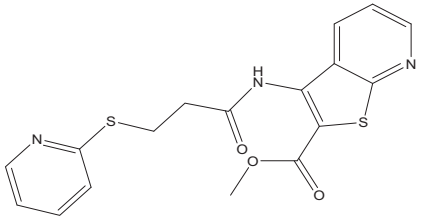	6.31
8	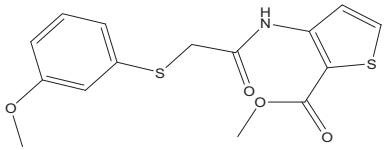	6.24
9	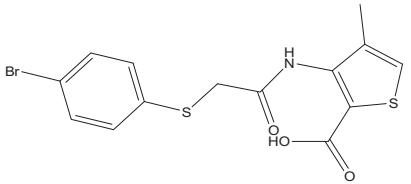	5.95
10	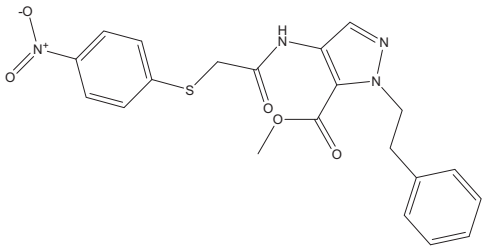	6.34
22	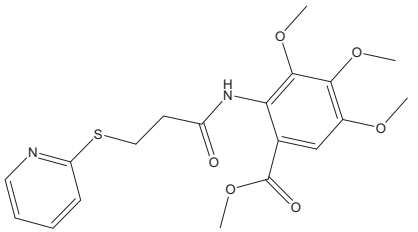	5.97
23	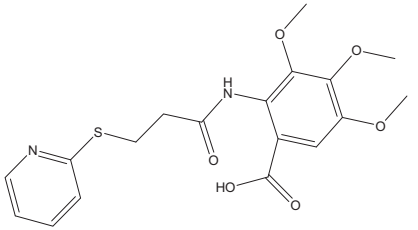	5.68
24	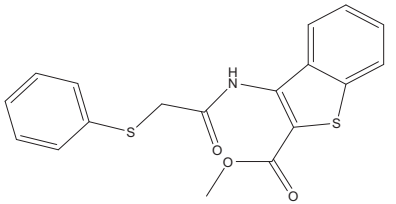	6.16
25	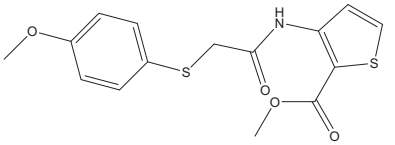	6.06
26	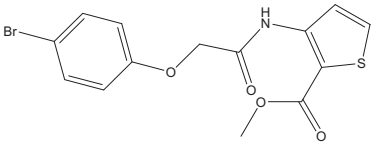	6.05

(*continued on next page*)

Table 1 (*continued*)

Compound	Structure	pEC_{50}	Compound	Structure	pEC_{50}
11	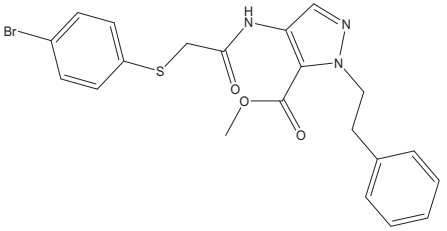	6.29	**27**	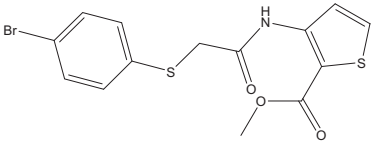	6.37
12	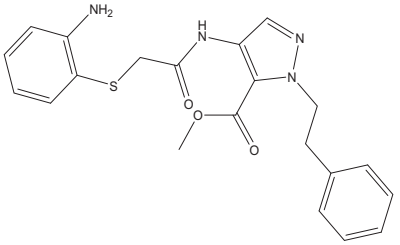	6.29	**28**	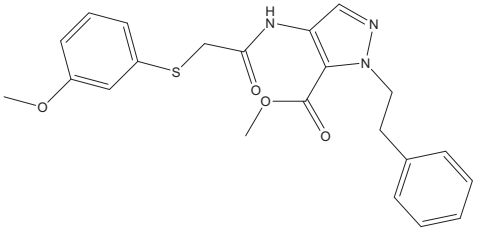	6.36
13	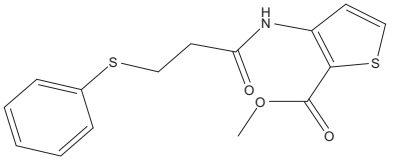	6.30	**29**	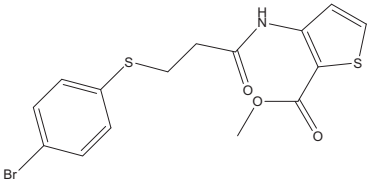	5.89
14	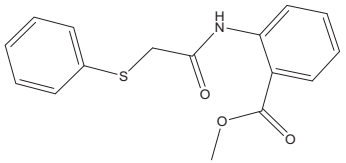	6.25	**30**	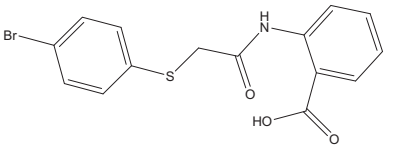	5.65
15	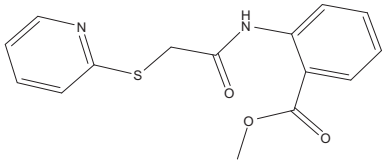	6.16	**31**	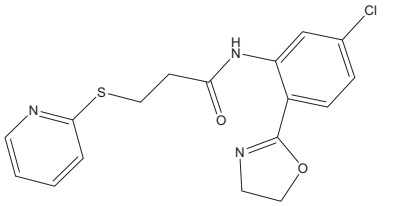	5.76
16	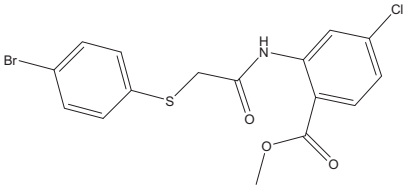	6.02	**32**	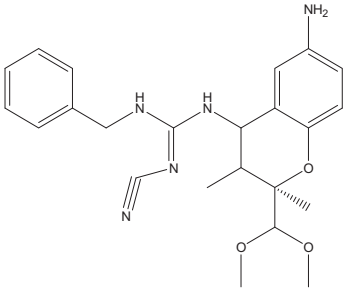	5.92

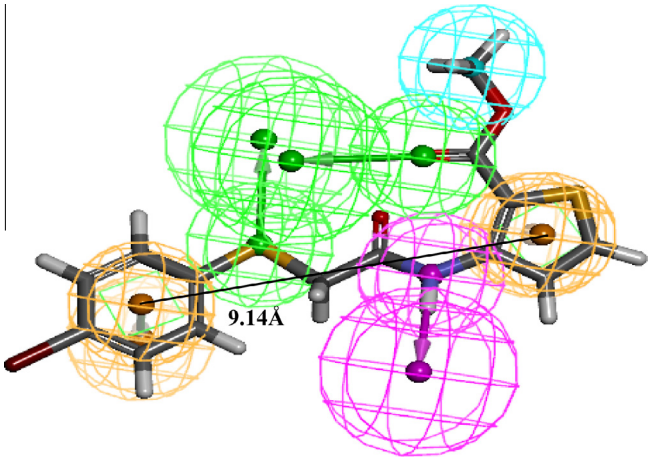

Figure 1. The pharmacophore mapping of the most active compound **27**. The pharmacophoric points are color coded with green; hydrogen-bond acceptor (HBA), magenta; hydrogen-bond donor (HBD), orange; ring aromatic (RA), Cyan; hydrophobic (HY).

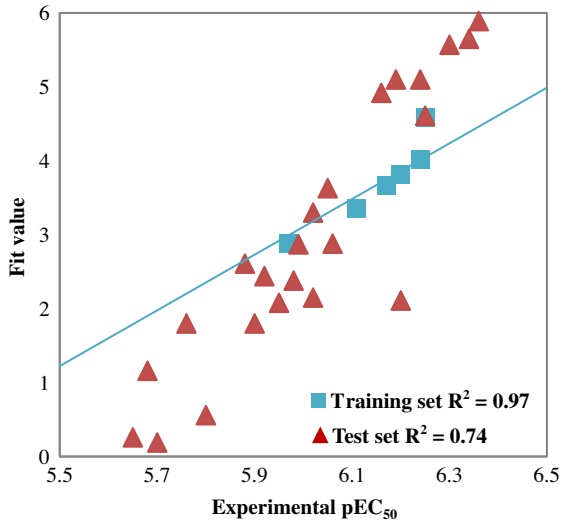

Figure 2. The relationship between experimental data versus pharmacophore fit value. Training set 7 compounds and test set 25 compounds. The correlation was calculated using spearman's correlation efficient.

Table 2
Summary of CoMFA and CoMSIA models

	CoMFA	CoMSIA
Statistical results		
q^{2a}	0.59	0.60
r^{2b}	0.98	0.97
SEE[c]	0.03	0.04
F value	142.78	94.28
components	6	6
Fraction (%)		
Steric	70.20	9.90
Electrostatic	29.80	16.90
Hydrophobic		40.10
Donor		15.70
Acceptor		17.40
Grid spacing: 2.0 Å		

[a] Cross validated correlation coefficient.
[b] Conventional correlation coefficient.
[c] Standard error of estimate.

The predictive power of the quantitative model was verified using the 25 compounds from the test data set. The best qualitative pharmacophore model contained six features: one hydrogen-bond donor (HBD), two hydrogen-bond acceptors (HBA), two ring aromatic features (RA), and one hydrophobic feature (HY), with each distance represented in Figure 1. This model had a maximum correlation coefficient of 0.97 with a high goodness of fit. Also, an independent test set that contained 25 external compounds was used to validate the established model and the obtained predictive score (0.74). The experimental and predicted activities of the training and test data set compounds are shown in Figure 2. The carboxylate group nearby the 2-position of the thiophene or the benzofuran ring indicated the importance of the hydrophobic group in conferring the biological activity. In contrast, when the carboxyl group was located in this region, it decreased the biological activity (e.g., compounds **9**, **18**, **23**, and **30**). This model proposes that the hydrophobic interactions between ligands and proteins are important. In order to clarify this further, the pharmacophore parameters of the training data set compounds are reported in Supplementary data Table 1.

The 3D-QSAR, CoMFA, and CoMSIA models were constructed using derivatives based on benzofuran analogues, as shown in Figure 3. Group 1 contains a training data set of 23 compounds that produce the 3D-QSAR model (compounds **1**–**23** in Table 1), and Group 2 is a test data set of 9 compounds (compounds **24**–**32** in Table 1) in order to validate the model. This model can be used

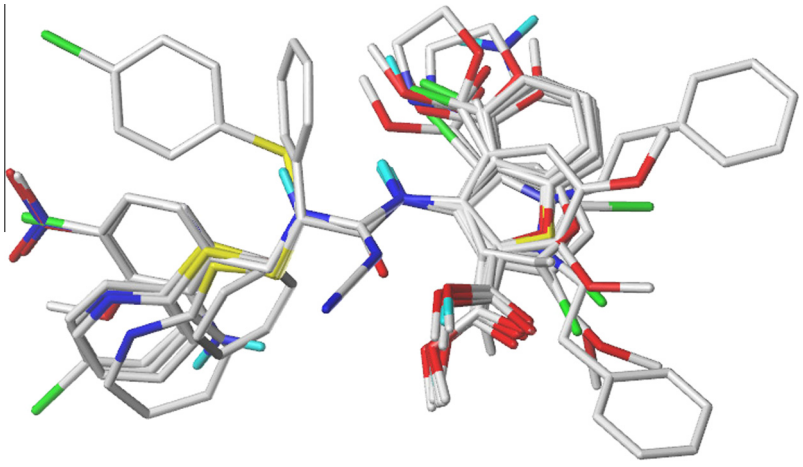

Figure 3. Stereo-view of the CoMFA/CoMSIA training and test set compounds superimposed in molecular shape analysis.

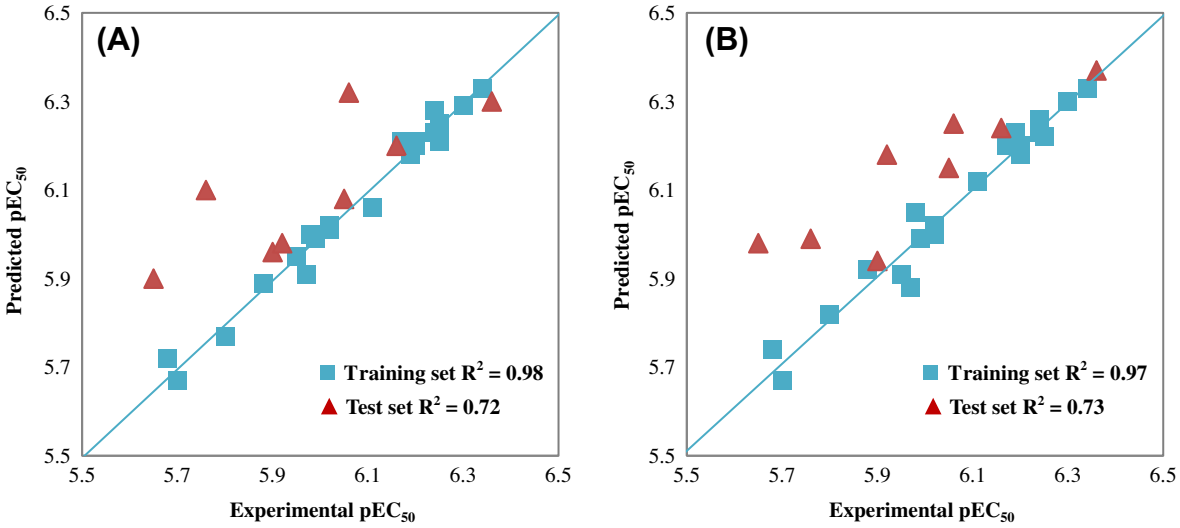

Figure 4. Plots of the experimental versus predicted pEC_{50} values of the training (■) and test (▲) compounds based on the best (A) CoMFA model and (B) CoMSIA model.

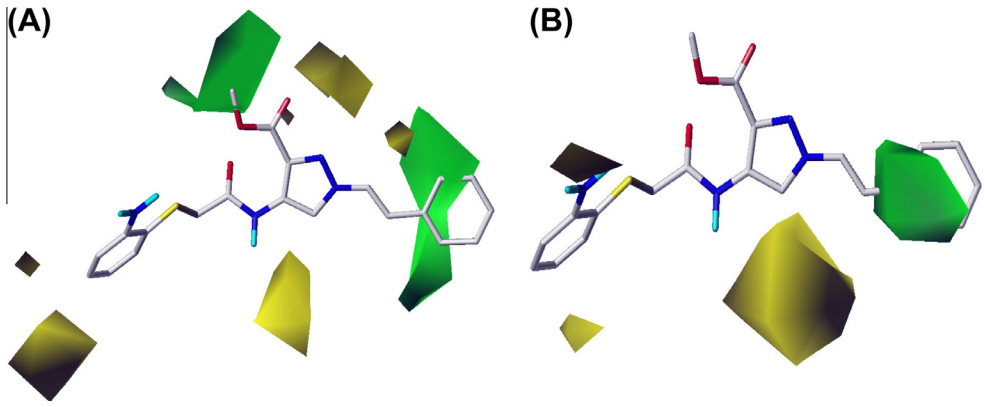

Figure 5. Contour maps of (A) CoMFA and (B) CoMSIA analysis based on compound **12**, high—scored conformation in training set. Green contours signify steric fields where bulky groups increase activity, while yellow contours indicate fields where less bulky groups decrease activity. CoMFA steric fields were displayed in favored level 80% (green) and disfavored level 20% (yellow), CoMSIA fields were in 85% and 15% contributions by using STDEV∗COEFF field. Compound **12** is depicted in capped stick type, referentially.

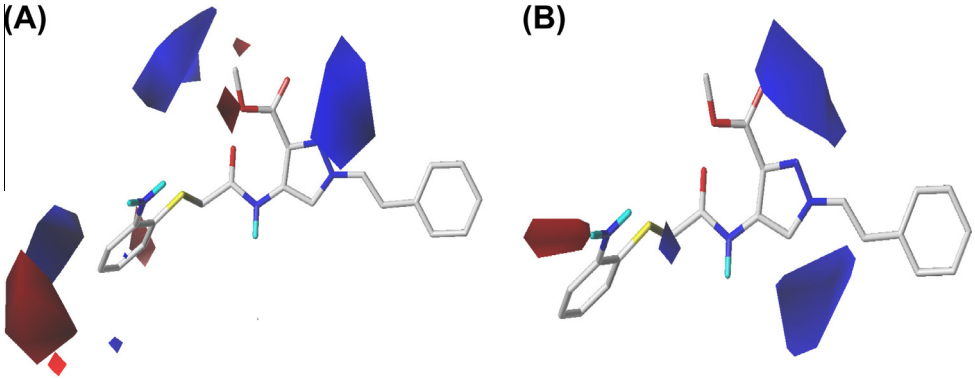

Figure 6. Contour maps of (A) CoMFA and (B) CoMSIA analysis are based on compound **12**. Blue contours signify electrostatic fields where positive charged groups increase activity, while red contours indicate fields where negative charged groups increase activity. CoMFA electrostatic fields were displayed in favored level 85% (blue) and disfavored level 15% (red), fraction of CoMSIA fields was identical.

to obtain numerical values for statistical results such as STDEV∗COEFF at individual lattice points. Partial atomic charges were calculated using the Gasteiger–Hückel charge.[12] The results were statistically significant and the data from the 3D-QSAR analyses are summarized in Table 2 and Figure 4. The best cross-validated LOO values for the CoMFA and CoMSIA models were computed as $q^2 = 0.59$ and $q^2 = 0.60$, respectively, using six components. The non-cross-validated values for the CoMFA and CoMSIA

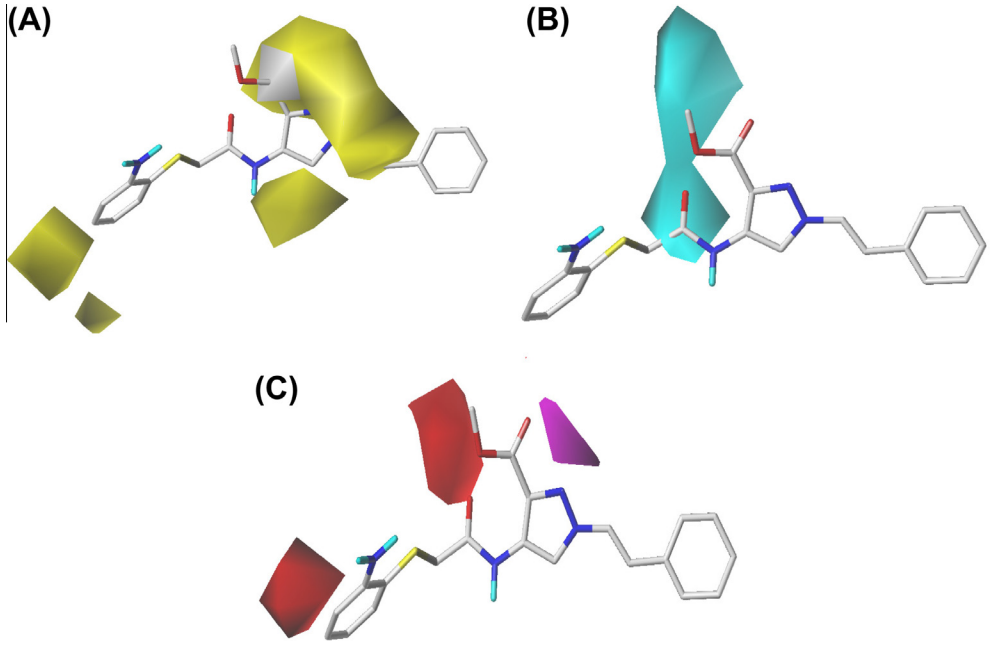

Figure 7. Contour map of CoMSIA analysis is based on compound **12**. Yellow and white contours (A) signify favorable and unfavorable hydrophobic fields in same proportion. Hydrogen bond donor contours (B) were displayed in favored level 75% (cyan) and disfavored level 25% (purple). And hydrogen bond acceptor contours (C) were indicated favorable fraction 90% (magenta) and unfavorable fraction 10% (red).

Table 3
Biological activity and predicted values of synthesized compounds

Compound	Structure	Cell death (%)	pEC_{50}	Fit value	CoMFA	CoMSIA
33	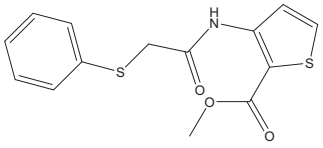	9.48	6.10	2.25	6.29	6.33
34	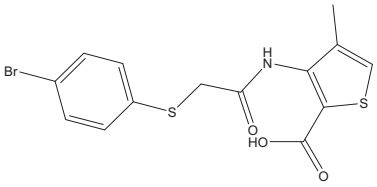	14.27	5.95	1.05	5.95	5.95
35	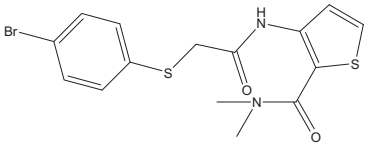	10.45	6.07	1.95	6.17	6.23
36	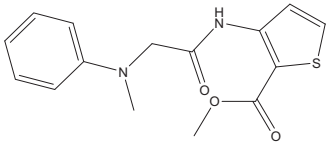	7.57	6.18	3.12	6.30	6.36
37	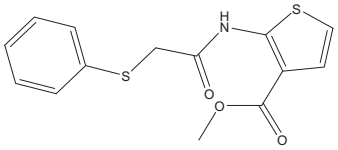	8.38	6.14	3.07	6.25	6.30

(*continued on next page*)

Table 3 (*continued*)

Compound	Structure	Cell death (%)	pEC_{50}	Fit value	CoMFA	CoMSIA
38	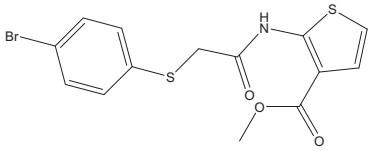	9.00	6.12	3.07	6.16	6.11
39	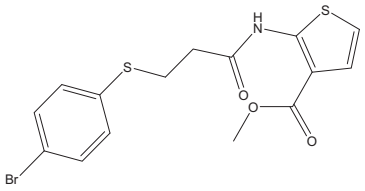	6.45	6.23	3.89	6.21	6.48
40	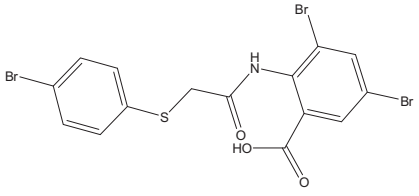	16.12	5.91	0.62	5.90	5.97
41	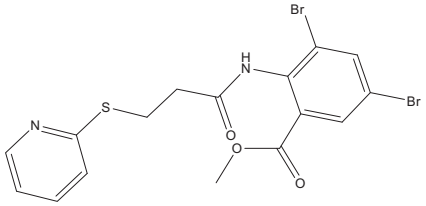	11.43	6.03	1.81	6.04	6.20
42	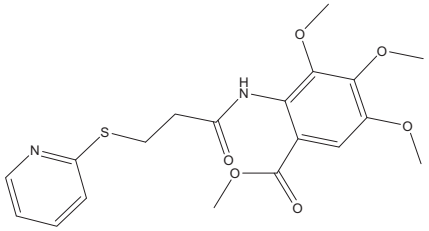	13.48	5.97	1.38	5.91	6.16
43	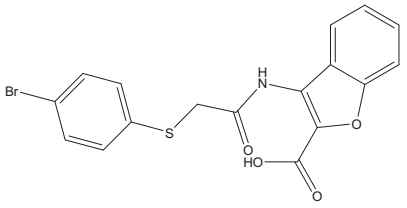	8.47	6.14	2.48	5.94	6.42
44	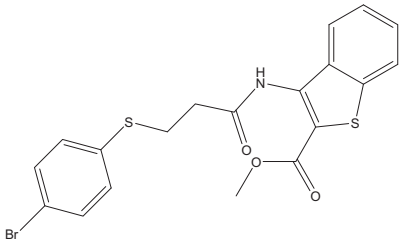	8.57	6.14	3.82	6.09	6.24
45	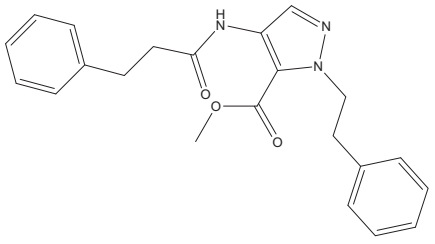	3.99	6.37	5.19	6.37	6.29

Table 3 (*continued*)

Compound	Structure	Cell death (%)	pEC_{50}	Fit value	CoMFA	CoMSIA
46	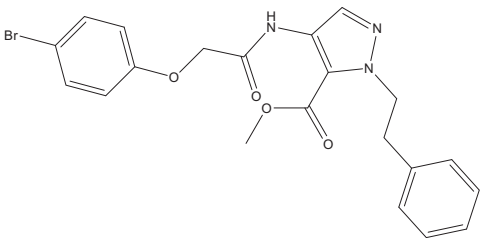	2.97	6.45	6.01	6.27	6.45

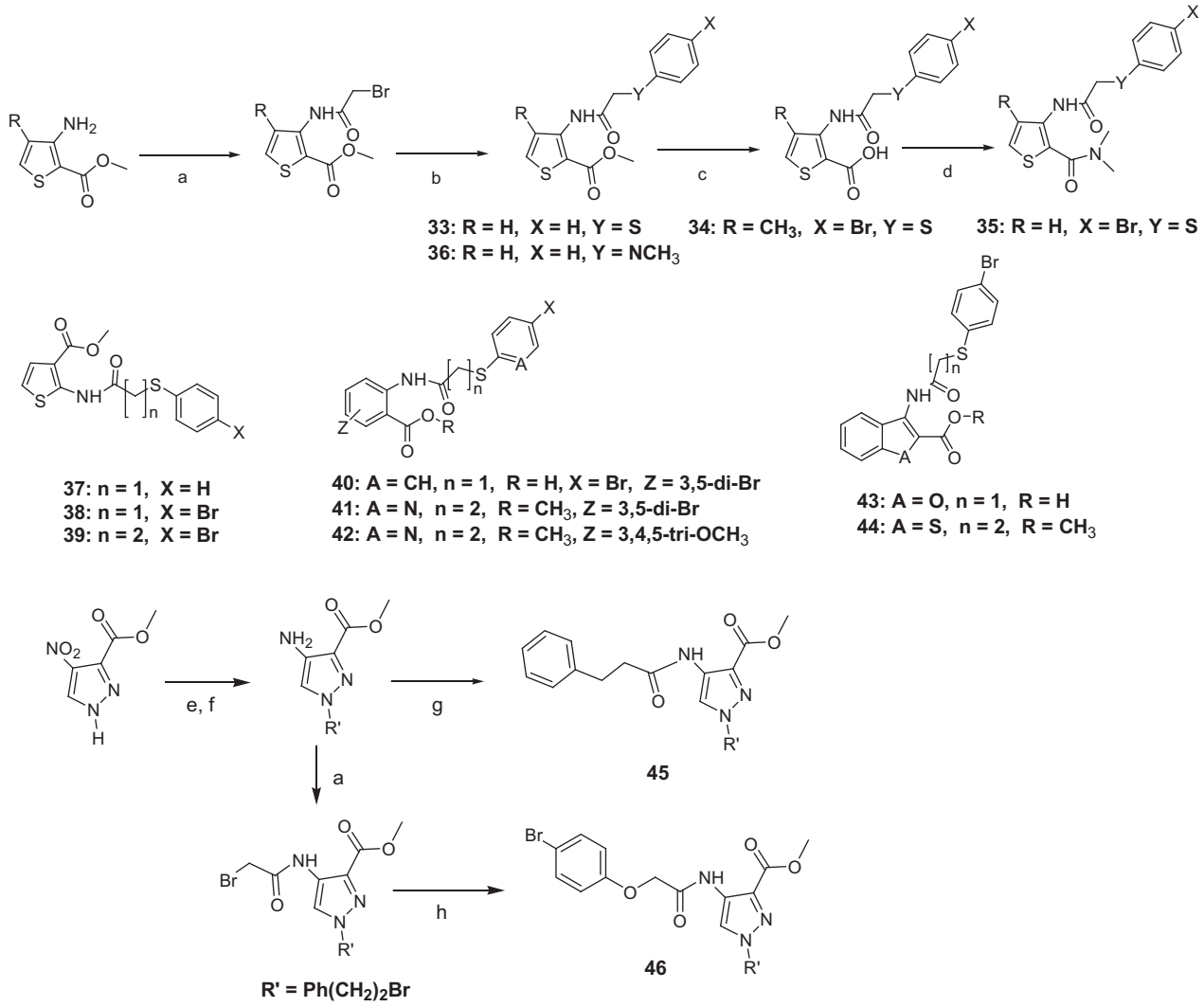

Scheme 1. Reagents and conditions: (a) bromoacethyl bromide, NEt_3, THF, rt, 83–93%; (b) (i) benzene thiol, NEt_3, THF, rt or (ii) *N*-methyaniline, K_2CO_3, DMF, rt, 42–91%; (c) 2 N NaOH, THF, reflux, 90%; (d) (i) di(2-pyridyl)carbonate, DMAP, THF, rt (ii) 40 wt % dimethylamine, rt, 50%; (e) (2-bromoethyl)benzene, Cs_2CO_3, DMF, rt, 74%; (f) H_2(g), 10% Pd/C, MeOH, 50 PSI, rt, 94%; (g) hydrocinnamoyl chloride, NEt_3, THF, rt, 87%; (h) 4-bromophenol, K_2CO_3, DMF, rt, 69%. And refer to Supplementary data for details.

models were calculated to be $r^2 = 0.98$ and $r^2 = 0.97$ with an estimated standard error of 0.03, 0.04 and *F* values of 142.78 and 94.28, respectively. The CoMFA and CoMSIA models were validated by substituting the test set compounds and obtaining sufficient prediction ($r^2_{predictive} = 0.72$ and 0.73, respectively).

The CoMFA and CoMSIA models were developed based on a superimposition obtained using the pharmacophoric map. The contours provide an interpretation of the correlation obtained in terms of the field contributions. The CoMFA model, which includes steric and electrostatic fields, is presented as 3D contour map using the STDEV∗COEFF field in Figure 5a and Figure 6a. The respective contributions of the steric and electrostatic fields for the CoMFA model are 70% and 30%. The green contours signify the steric fields where the bulky groups increase activity, while the yellow contours indicate fields where the less bulky groups decrease activity. As mentioned above, the green contours shown near the

meta-position of the benzofuran signify that any bulky group at this site could increase activity. The yellow contours near the 4′-position of the benzene ring suggest that any bulky group could decrease activity. Compounds **14** and **25** showed a negative relationship between the predicted pEC_{50} and the character of the contours. The blue contours signify electrostatic fields where positively charged groups increase activity, while the red contours indicate fields where the negatively charged groups increase activity. Compounds **1** and **10** were accurately interpreted as red contours; thus, nitro-benzene, which contains a negative group, had the highest activity.

Similar to the CoMFA fields, the CoMSIA model was also developed using the STDEV∗COEFF field, as shown in Figure 5(b), Figure 6(b), and Figure 7. The respective contributions of the steric and electrostatic fields for the CoMSIA model were 10% and 17%. The CoMSIA fields were aligned similarly to the CoMFA fields. In addition, the CoMSIA model contained hydrophobic, hydrogen-bond donor, and hydrogen-bond acceptor fields. The respective contributions of these three fields were 40%, 16%, and 17%. In the hydrophobic contour map, the yellow contours indicate the sites where the hydrophobic groups are favorable and the white contours show unfavorable positions. In Figure 7a, the two yellow contours are located in the vicinity of the benzofuran and amine groups, which signify that the hydrophobic groups facilitate higher activity. Compounds **10**–**12** are well fitted to our model, which had highly predictive ability. The yellow contours near the 1′-position of the pyrazole ring suggest that any hydrophobic substitution could increase activity. In the hydrogen bond donor contour map, the cyan contours indicate the regions where the hydrogen bond donor groups are favorable and the purple contours show unfavorable positions in Figure 7(b). Figure 7(c) depicts the hydrogen bond acceptor contour map. The magenta contours indicate the sites where the hydrogen bond acceptor groups are favorable for activity, while the red contours present the regions where hydrogen bond acceptors are unfavorable. Herein, all contour maps were depicted with compound **12** in Figures 5–7.

Based on the well-accepted pharmacophore and 3D-QSAR models, the 14 new compounds shown in Table 3 were designed and synthesized in order to predict accurate activities, as presented in Supplementary data Table 2. Based on our computational modeling and investigation of the SAR, two aromatic features were key points in the biological activity. According to Figure 1, the distance between two RA central points was 9.14 Å and we synthesized 14 novel compounds with a carbon linker ($n = 4, 5$) while adhering to the distance rule. For this reason, the thiophene and pyrazole derivatives were synthesized from the corresponding 3-amino-thiophene-2-carboxylic acid methyl ester and 4-nitro-pyrazole-3-carboxylate as readily available starter materials, as described in Scheme 1 and the Supplementary data. The following compounds were prepared according to the general procedures described above employing the appropriate methyl 3-aminothiophene-2-carboxylate, benzenethiol, and pyrazole. The modification of the aromatic ring or benzofuran core was achieved using a similar method as described for the synthesis of compound **33**. Following these procedures, numerous analogues (e.g., benzofuran and benzene derivatives) were prepared in a short period in a parallel synthesis fashion. Consequently, the 14 synthesized compounds were well-matched with two key ring aromatic centers and they obtained reasonable fitted values compared with the experimental activity, as summarized in Table 3.

In summary, this study developed pharmacophore and 3D-QSAR models for analogues of 3-substituted-benzofuran-2-carboxylic ester as inhibitors of the Fas-mediated cell death pathway. The proposed pharmacophore model has good agreement with the synthesized compounds and is capable of explaining the variance in biological activities coherently with respect to the structures of the data set compounds. The predictive power for the synthesized compounds was 0.96 for the pharmacophore model, 0.58 for the CoMFA model, and 0.57 for the CoMSIA model. Consequentially, the prediction of the ligand-based pharmacophore hypothesis provided significant structural insights and also illuminated the important binding features of heterocyclic–carboxylic ester analogues. In future research, we will develop strategies for the optimization of the inhibitors of the Fas-mediated cell death pathway based on these results.

Supplementary data

Supplementary data associated with this article can be found, in the online version, at http://dx.doi.org/10.1016/j.bmcl.2013.07.018.

References and notes

1. Hearse, D. J. *Cardiovasc. Res.* **1994**, *28*, 1737.
2. Margaix Muñoz, M.; Jiménez Soriano, Y.; Poveda Roda, R.; Sarrión, G. *Med. Oral. Patol. Oral. Cir. Bucal.* **2008**, *13*, E296.
3. Ryu, S. W.; Chae, S. K.; Lee, K. J.; Kim, E. H. *Biochem. Biophys. Res. Commun.* **1999**, *262*, 388.
4. Menges, C. W.; Altomare, D. A.; Testa, J. R. *Cell Cycle* **2009**, *8*, 2528.
5. Suh, J. H.; Yi, K. Y.; Lee, Y. S.; Kim, E. H.; Yum, E. K.; Yoo, S. E. *Bioorg. Med. Chem. Lett.* **2010**, *20*, 6362.
6. Cramer, R. D.; Patterson, D. E.; Bunce, J. D. *J. Med. Chem. Soc.* **1988**, *110*, 5959.
7. Klebe, G.; Abraham, U.; Mietzner, T. *J. Med. Chem.* **1994**, *37*, 4130.
8. Kim, S. O.; Cho, I. S.; Gu, H. K.; Lee, D. H.; Lim, H.; Yoo, S. E. *Eur. J. Pharmacol.* **2004**, *487*, 81.
9. Suh, J. H.; Yoo, S. E.; Yi, K. Y.; Kim, N. J.; Kim, E. H.; Jung, Y. S.; Lee, Y. S.; Kim, H. Y. Patent PCT WO 20,09,048,274, 2009.
10. Barnum, D.; Greene, J.; Smellie, A.; Sprague, P. *J. Chem. Inf. Comput.* **1996**, *36*, 563.
11. Hecker, E. A.; Duraiswani, C.; Andrea, T. A.; Diller, D. J. *J. Chem. Inf. Comput.* **2002**, *42*, 1204.
12. Gasteiger, J.; Marsili, M. *Tetrahedron* **1980**, *36*, 3219.